



Experimental and Numerical Simulation for Thermal Investigation of Oscillating Heat Pipe Using VOF Model

Anwar S. Barak ^{a*}, Ahmed A. M. Saleh ^b, Zained H. Naji ^c

^a University of Technology, Baghdad, Iraq, anwar.barrak@yahoo.com

^b University of Technology, Baghdad, Iraq, aamsaleh60@gmail.com

^c University of Technology, Baghdad, Iraq, 20082@uotechnology.edu.iq

*Corresponding author.

Submitted: 05/05/2019

Accepted: 10/08/2019

Published: 25/1/2020

KEY WORDS

Pulsating heat pipe, filling ratio, two phase flow, heat flux, and Standard k- ϵ model.

ABSTRACT

This study is investigated the thermal performance of seven turns of the oscillating heat pipe (OHP) by an experimental investigation and CFD simulation. The OHP is designed and made from a copper tube with an inner diameter 3.5 mm and thickness 0.6 mm and the condenser, evaporator, and adiabatic lengths are 300, 300, and 210 mm respectively. Water is used as a working fluid with a filling ratio of 50% of the total volume. The evaporator part is heated by hot air (35, 40, 45, and 50) °C with various face velocity (0.5, 1, and 1.5) m/s. The condenser section is cold by air at temperature 15 °C. The CFD simulation is done by using the volume of fluid (VOF) method to model two-phase flow by conjugating a user-defined function code (UDF) to the FLUENT code. Results showed that the maximum heat input is 107.75 W while the minimum heat is 13.75 W at air inlet temperature 35 °C with air velocity 0.5m/s. The thermal resistance decreased with increasing of heat input. The results were recorded minimum thermal resistance 0.2312 °C/W at 107.75 W and maximum thermal resistance 1.036 °C/W at 13.75W. In addition, the effective thermal conductivity increased due to increasing heat input. The numerical results showed a good agreement with experimental results with a maximum deviation of 15%.

How to cite this article: A. S. Barak, A. A.M. Saleh and Z. H. Naji, "Experimental and Numerical Simulation for Thermal Investigation of Oscillating Heat Pipe Using VOF Model" Engineering and Technology Journal, Vol. 38, Part A, No. 1, pp. 88-104, 2020.

DOI: <https://doi.org/10.30684/etj.v38i1A.286>

This is an open access article under the CC BY 4.0 license <http://creativecommons.org/licenses/by/4.0/>.

1. Introduction

Oscillating heat pipe (OHP) is one of a unique type of heat pipes, which can consider a promising heat transfer devices used in the case of high heat transfer rate in micro-spaces [1].

Oscillating heat pipe OHP is the kind of two-phase heat transport devices that rely on phenomena of the oscillatory flow of liquid slug and vapor bubble in a long capillary tube and a small diameter

range from 0.1 mm to 5 mm bent into many turns. OHP structure comprised of evaporator section, adiabatic section and condenser section are located at these turns. The OHP had many features compared to the conventional heat pipe such as simplicity and OHP has no wick structure [2,3]. The long tube meandering of the OHP results in unstable vapor bubbles in its evaporator section where heat is added to the working fluid, so vapor pressures at neighboring tube sections led to an oscillating flow of working fluid. Therefore, heat transfer rate will be enhanced between evaporator and condenser sections and OHP can achieve very high effective thermal conductivity up to 10,000 W/m °C [4]. Due to the high ability of OHP to transport heat, the OHPs can be used in a wide engineering application including air-to-air heat exchanger to recover waste heat in HVAC system, steam power plants, and in variety of industrial heat recovery applications [5].

Jiao et al. [6], investigated the heat transfer and transport capacity of horizontal OHP in the cryogenic environment by using liquid nitrogen as working fluid. They used 8-turn copper OHP with inner diameter 1.65 mm and lengths of evaporator section, adiabatic section, and condenser section is 40, 100, and 60 mm respectively. The heat input at evaporator changed from 20.5 W to 380 W. The results showed that the operation of OHP may be divided to unsteady region, transient region, and a new steady state region and thermal resistance reduction from (0.256 – 0.112) when input heat raised from (22.5 – 321.8) W. The binary fluid is used in OHP [7]. They used closed-loop OHP consist of 5 turns fabricated from copper. Inner diameter was 2 mm and the height of the evaporator section, adiabatic section, and condenser section were 80 mm, 10 mm, and 90 mm respectively. The working fluids with filling ratio 60% that used in OHP were pure fluids (water, methanol, ethanol, and acetone) and binary fluids with a 1:1 volume-mixing ratio. The results showed the binary fluids had a low thermal resistance. The effects of inclination angle, filling ratio, operating temperature, working fluid, and evaporator length on heat flux are investigated [8]. They used in their study closed loop OHP with a check valve (CLOHP/CV) had a 40 turns with the inner diameter 2.03 mm and 2 check valves. The filling ratios were (30%, 50%, and 80%) by total volume, working temperatures were (45, 55, and 65) °C, the working fluids were (pure water, ethanol, and R123), and inclination angles were (20°, 40°, 60°, 80° and 90°). The results showed that max heat flux achieved at filling ratio of 50% for all cases, R123 experience higher heat flux than ethanol and water due to the low boiling point, and heat flux decreased with increasing of evaporator length. OHP as a heat exchanger in HVAC system was used by [9]. They tested copper tube ten turns of OHP with inner diameter 1.65mm and the empty OHP and partially filled with n-pentane by filling ratio 70% by total volume were considered. The evaporator section was heated by air at temperature 45 °C and the condenser section was cold by air at 6 °C with constant volumetric ratio 0.19 m3/s. The results showed that the thermal effectiveness were 0.064, 0.05, and 0.02 for theoretical, filled with n-pentane, and empty OHP respectively. While the recovered heat was 240 W. Rahman et al. [10] experienced finned and un-finned tubes in the structure of OHP made from copper tube meandering in 8 turns with inner diameter 2.5mm and outer diameter 3mm. The length of the evaporator, adiabatic, and condenser sections were 50, 120, and 80mm respectively. The copper wires with 1 mm diameter used as fins inserted along only in condenser section at an equal distance between fins. Methanol and Ethanol fluids were used as working fluids with a 50% filling ratio. The heat input at three inclination angles (0, 30, and 45) degree. The evaporator section was insulated and heated by the heater at (10 – 80) W, while the condenser section was cooled by forced air. The results showed that Methanol had lower thermal resistance than Ethanol, and finned – inserted structure showed better performance than the un-finned structure.

The traditional smooth and micro-grooved tubes OHP were investigated by [11]. They fabricated copper OHP with three turns and the length of evaporator, adiabatic, and condenser sections were 70, 230 and 110 mm, respectively. The internal diameters for a smooth tube were 4 mm and 4.8 mm and the internal diameter of OHP with adding a helical micro-grooved structure on the inner wall was 4.5 mm. The working fluid was water by filling ratio of 50% by volume. The obtained results indicated that adding micro-grooved can enhance the thermal performance of OHP by increase the heat transfer rate, reduce the thermal resistance, and increase the thermal conductivity.

Nazaria et al. [12] studied the effect of adding nanofluid to water as based fluid in the thermal performance of an OHP. They used copper OHP with inner diameter 2 mm and 2 turns. Graphene oxide was used as nanofluid in four concentrations added to water to use as working fluid by 50 % filling ratio of total volume. The results showed that adding graphene oxide nanosheets to water can enhance the thermal performance of OHP by decreasing the thermal resistance by more than 40 % in comparison to pure water.

A many of simulating models have been developed recently to predict the oscillating motion and heat transportation performance in the OHP. Z. Lin et al [13] built the CFD model using a mixture and VOF method to model the operation and predict the heat performance of 4 turns copper miniature OHP. The experimental semi visualized and thermal performance apparatuses were conducted to verify the models. They found the thermal performance could be enhanced when the inner diameter of MOHPs was increased. CFD code used by Nagwase et al. [14] with a selection of the VOF method for studying the motion of working fluid and predict thermal performance in OHP. Star CCM+ solver and CSF model were considered to study the effect of surface tension. The semi visualized 2 turns OHP was used with inner diameter 2 mm filled with water by 60% filling ratio. The results showed that the VOF model provides a good agreement with experimental work with variation about (5 – 10) %.

The aim of this paper is to investigate the thermal performance and predicted the flow behavior of OHP used water as working fluid by experimental and numerical CFD model. The experimental part of this study has been done to investigate the thermal performance of seven turns OHP fabricated from copper. The various inlet air temperatures and velocities are recorded for analyzing the thermal resistance and thermal conductivity of the OHP. While the numerical part, The CFD code based on the volume of fluid (VOF) method was used. Turbulent flow is assumed based on the standard ($k - \epsilon$) model to have accurate predict of the internal flow behavior and the thermal performance of the OHP.

2. Experimental Apparatus

The schematic diagram of OHP with thermocouples positions is shown in Figure 1. OHP with measurement devices and data acquisition systems were used to achieve the experiments of this study as shown in Figure 2. OHP was designed and fabricated from copper bending to 7 turns with a length of the evaporator, adiabatic, and condenser sections 300, 210, 300 mm respectively. The OHP filled partially by working fluid (water), with a filling ratio of 50%. This is due to water is suitable working fluid for temperatures between 30°C and 300°C, and have good compatibility with various metals like copper and stainless steel and the active oscillating flow and maximum velocity of circulation of working fluid can be achieved at charging ratio 40 – 60 % [15, 16]. The evaporator section heated by air at temperature (35, 40, 45, and 50) °C with face velocity (0.5, 1, 1.5) m/s respectively. The air temperature is supplied and controlled by the heater system. The air face velocity is controlled by using variable AC transformer (variac), of an output ratio ranges from (0 to 100%) of the input voltage. While the condenser section of OHP is cooled by air at 15°C using air condition system. The mass of the airflow rate is equal for both sections (evaporator and condenser). The adiabatic section was well insulated by using fiberglass insulation to prohibit heat loss. Fourteen (K-Type) thermocouple calibrated with accuracy 0.05 °C were used with data acquisition to measure the average wall temperature of OHP sections and air temperatures. A hot wire anemometer used to measure air velocity with accuracy ±0.2 m/s. The vertical bottom heat mode condition is conducted for all the tests.

3. Experimental Calculation

The heat input in the evaporator section is equal [17].

$$Q_{in} = m \cdot C_p (T_i - T_o) \quad (1)$$

Where Q_{in} is the heat input (W), T_i and T_o are the air temperatures at inlet and exit of evaporator section as shown in Figure 3.

The thermal resistance (°C/W) of OHPs is calculated by the equation below [18].

$$R_{th} = \frac{\bar{T}_{ev} - \bar{T}_{co}}{Q_{in}} \quad (2)$$

The effective thermal conductivity of OHP is calculated as [19].

$$K_{eff} = \frac{Q_{in} \times L_{eff}}{N \times A_{cross} \times (\bar{T}_{ev} - \bar{T}_{co})} \quad (3)$$

Where R_{th} is the thermal resistance (°C/W). K_{eff} is effective thermal conductivity in (W/m.K), \bar{T} is wall average temperature value is measured at evaporator section and condenser section N is number of tubes of the evaporator section, and A_{cross} is cross-sectional area of the OHP. The effective length can be [20]:

$$L_{eff.} = 0.5 (L_e + L_c) + L_a \quad (4)$$

Where L_e , L_c , and L_a is the length of evaporator, condenser, and adiabatic section respectively.

4. Simulation Model

The literature survey showed there is no theoretical simulation successfully predicted thermal performance of the OHP. This is due to the chaotic phenomena of OHP which result the internal flow and heat transfer by pulsation process are complicated to model. Also, for best knowledge of the researcher that there is no literature using VOF method turbulent ($k - \varepsilon$) model. So in this work, turbulent standard ($k - \varepsilon$) model is used to gain accurate theoretical result but it consuming longer time in run solution than laminar approach.

I. Physical model

A simulated of two dimensional was modified to model the two phase flow and heat transportation process in the oscillation heat pipe. The heat pipe model constructed with inner diameter 3.5 mm and the length of evaporate, condenser, and the adiabatic sections were 300, 300, 210 mm respectively. The OHP with 7 turns filled partially by water with filling ratio 50% from the total volume. First the geometry is created with total length 810 mm and then meshed as shown in Figure 4. The mesh grid had 78% quality with minimum and maximum size were 5×10^{-4} m and 2×10^{-3} m respectively.

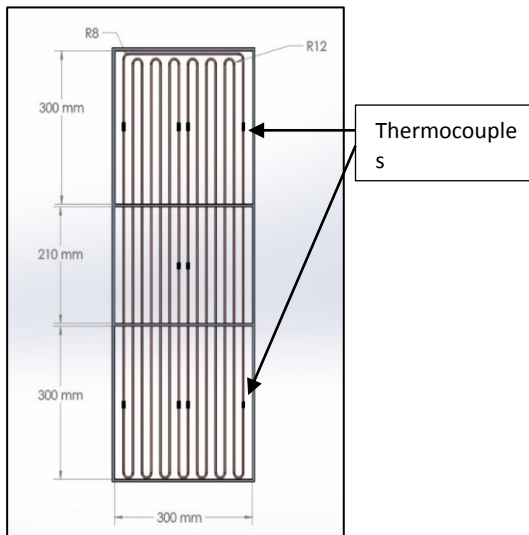


Figure 1: Schematic and photo image of 7 turns of copper OHP

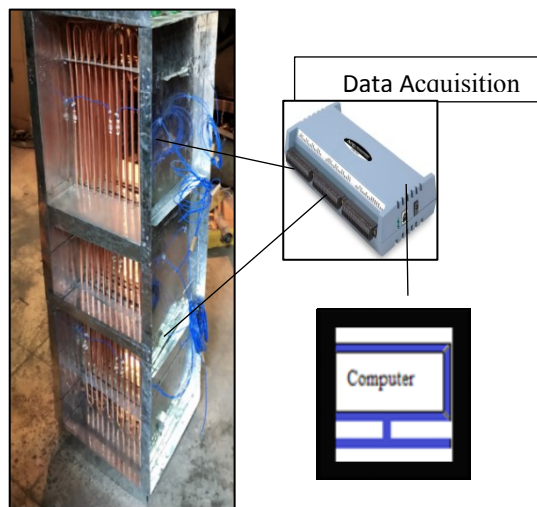


Figure 2: Photograph of 7 turns of copper OHP

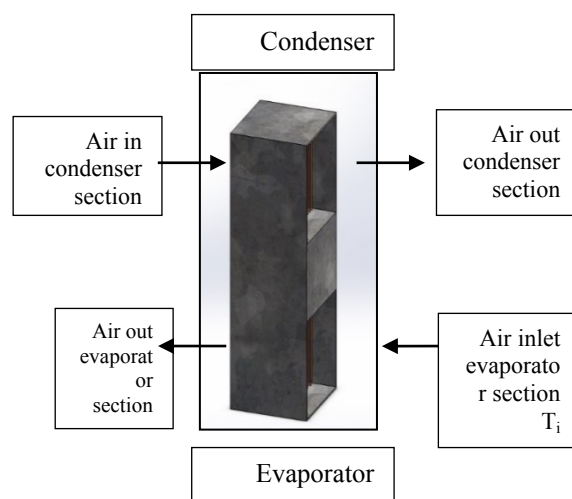


Figure 3: Air flow diagram

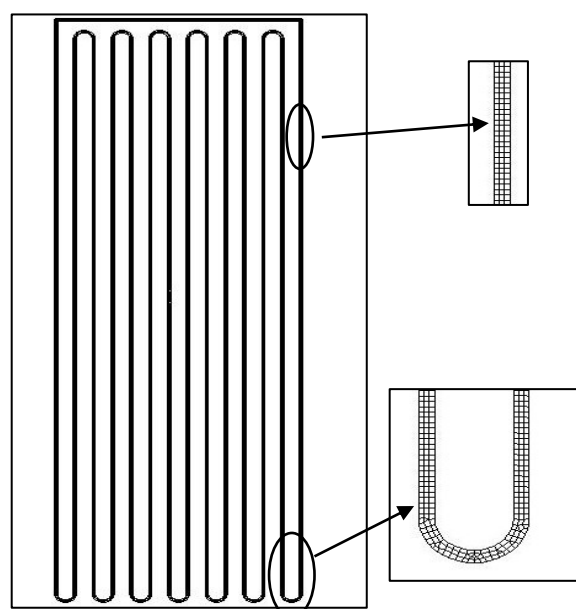


Figure 4: Mesh grid generation of OHP

II. Mesh quality and dependency

The independent test is important to know how many cells are used for simulation flow which does not affect on the numerical result. The results accuracy will increase with increasing the number of cell mesh but at a certain number because the greater mesh number takes a long time to reach the output results. Figure 5 shows a grid independence test to ensure that the mesh modification does not affect the numerical results by means of the Courant number (the ratio of the time step to the time that a fluid takes to move across the cell). Table 1 presents the mesh properties.

Table 1: Mesh properties

Cell Type	Cell Size (m)	No. of cells	No. of nodes
Quadrilateral	0.0004	52000	64600

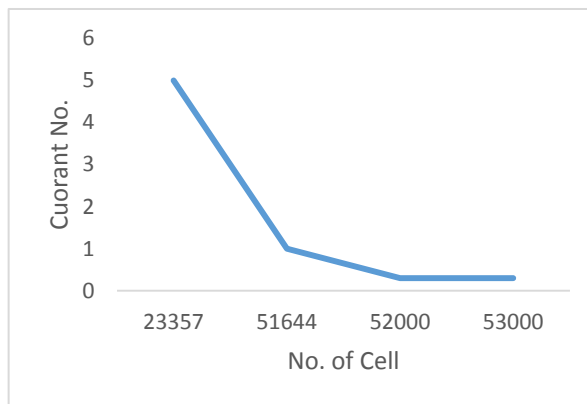


Figure 5: Courant number during mesh testing

III. Mathematical model and governing equations

Volume of fluid (VOF) approach was chosen to characterize motion of working fluid in OHP with equations of continuity, momentum, and energy respectively. The process of phase change of the working fluid in OHP used in this work can be inserted and interpreted for each phase a file of user defined function code (UDF).

1) Volume of fluid (VOF)

The simulation of two or more homogeneous mixture of fluids can be done by using Volume of Fluid method by finding solution to a one group of momentum equation and tracking the volume fraction of every fluid through the domain. This method can be classified under to the kind of Eulerian technique which can be applied to trace and locate the interface between fluids. Volume of fluid model based on there is no interpenetrating between two (or more) fluids (phases). For all phases in every control volume in the computational cell, the volume fraction sum to unity and variable must be introduced. So the volume fraction of every phase is defined at every location and all variables and properties of fluids are shared by the phases and represent volume- averaged values. This means depending upon the values of volume fraction, the variables and the properties in each given cell are either represented by one of the phases, or represented by a mixture of the phases. If the volume fraction of fluid in the cell is denoted as α_q , there are three possible conditions as:

- $\alpha_q = 0$ (liquid phase).
- $0 < \alpha_q < 1$ (mixture cell have interface between one (or more) fluid phases).
- $\alpha_q = 1$ (empty cell).

2) Governing Equations

A. Continuity Equation

To complete the tracking of interface(s) between the phases is done by solve an equation of continuity for the volume fraction of the phase(s). The equation of continuity for the q^{th} phase will be [21]:

$$\frac{\partial \alpha_q}{\partial t} + \vec{v} \cdot \nabla \alpha_q = - \frac{s_m}{\rho_q} \quad (4)$$

$$\sum_{q=1}^n \alpha_q = 1 \quad (5)$$

Where (v): the velocity, ρ : the density, t : the time, and S : the source term of mass with assumption that the phase change is occurred in the saturation temperature.

The volume equation can be resolved by using explicit time scheme.

In this work the explicit time scheme is used as follows.

$$\frac{\alpha_q^{n+1} \rho_q^{n+1} - \alpha_q^n \rho_q^n}{\Delta t} V + \sum_f (\rho_q U_f^n \alpha_{q,f}^n) = \left[\sum_{p=1}^n (m_{pq} - m_{qp}) + S_{\alpha_q} \right] V \quad (6)$$

Where

$n+1$: new (current) time step index.

n : previous time step index.

α_q^{n+1} : The volume fraction value at time step $n+1$.

α_q^n : The volume fraction value at time step n .

$\alpha_{q,f}^n$: The Face volume fraction value of the q^{th} .

V : Cell volume.

U_f^n : Volume flux through the face, based on normal velocity.

B. Momentum Equation

A one momentum equation was resolved during the field, and the velocity field result is shared during the phase. The momentum equation is dependent on the volume fractions of all phases during the properties ρ and μ [21].

$$\frac{\partial \rho \bar{v}}{\partial x} + \nabla \cdot (\rho \bar{v} \bar{v}) = -\nabla p + \nabla \cdot \left[\mu (\nabla \bar{v} + \nabla \bar{v}^T) - \frac{2}{3} \mu \nabla \cdot u I \right] + \rho \bar{g} + F_{CSF} \quad (7)$$

Where the pressure represented by P is, the dynamic viscosity represented by μ , the acceleration of gravity represented by g , the surface tension represented by F_{CSF} is, and the tensor represented by I .

In the above equation, the forces acting on the fluid and the surface tension force phases are included at the interface between two phases. J.U Brackbill et al [22] modeled the continuum surface force (CSF) and they proposed the following formula:

$$F_{CSF} = \sigma_{lv} \frac{\alpha_l \rho_l k_v \nabla \alpha_v + \alpha_v \rho_v k_l \nabla \alpha_l}{0.5 (\rho_l + \rho_v)} \quad (8)$$

Where;

$$k_l = \frac{\Delta \alpha_l}{\nabla \alpha_l}, k_v = \frac{\Delta \alpha_v}{\nabla \alpha_v}, \quad (9)$$

$$\mu = \alpha_l \mu_l + \alpha_v \mu_v \quad (10)$$

C. Energy Equation

The energy equation will be [21]:

$$\begin{aligned} \frac{\partial}{\partial t} (\rho e) + \nabla \cdot (\rho e \bar{u}) &= \nabla \cdot (k \cdot \nabla T) + \nabla \cdot (p \bar{u}) \\ &+ S_E \end{aligned} \quad (11)$$

Where

$$\rho = \alpha_l \rho_l + \alpha_v \rho_v \quad (12)$$

$$k = \alpha_l \rho k_l + \alpha_v \rho k_v \quad (13)$$

$$e = \frac{\sum_{q=1}^n \alpha_q \rho_q e_q}{\sum_{q=1}^n \alpha_q \rho_q} \quad (14)$$

$$e = \frac{\alpha_l \rho_l e_l + \alpha_v \rho_v e_v}{\alpha_l \rho_l + \alpha_v \rho_v} \quad (15)$$

Where e and k are represented the energy and the coefficient of thermal conductivity, respectively and

$$e_L = C_{p,l} (T - T_{sat}) \quad (16)$$

$$e_V = C_{p,v} (T - T_{sat}) \quad (17)$$

T temperature and T_{sat} saturation temperature, and C_p is specific heat capacity. S_E is the energy source due to phase change.

IV. Evaporation and condensation process

Through the process of evaporation and condensation, the process of mass and heat transfer can be defined by using the user defined function (UDF). UDF was contacted with FLUENT code to complete the process of evaporation and condensation by calculation mass and heat transfer between two phases. S.C.K. De Schepper et al [23] suggested source terms used for determining the required mass and heat transfer to complete this process.

For mass transfer: the source term in Eq. 4 can be calculated as below:

Evaporation process:

$$S_{m,lv} = \begin{cases} -0.1 \frac{\alpha_v \rho_v (T_l - T_{sat})}{T_{sat}} & T_l > T_{sat} \\ 0 & T_l < T_{sat} \end{cases} \quad (18)$$

Condensation process

$$S_{m,vl} = \begin{cases} 0.1 \frac{\alpha_v \rho_v (T_{sat} - T_v)}{T_{sat}} & T_v < T_{sat} \\ 0 & T_v > T_{sat} \end{cases} \quad (19)$$

For heat transfer: the source term in Eq. 11 can be calculated as below:

$$S_{E_{lv}} = S_{m,lv} LH \quad (20)$$

$$S_{E_{vl}} = S_{m,vl} LH \quad (21)$$

And LH: latent heat of evaporation process.

V. Boundary conditions

The predict of evaporation and condensation process done with assumption no slip boundary condition at the inner wall of OHP and adiabatic section is well insulated so there is no heat flux at this section. The evaporator section is heated at 40°C, while the condenser section is cooled at constant temperature 15 °C. The liquid slug and vapor plug begun to form when the operation is stated and the solution may be reached to the steady state after 60s.

VI. Solution approach

The standard k - ε standard turbulent scheme is chosen to solve this transient case with selection of enhance wall temperature, thermal effective, and curvature correction solvers. In addition, the pressure-velocity conjugation is resulted by the semi-implicit approach into pressure related equations (SIMPLE) algorithm. The pressure staggering option (PRESTO) scheme is selected into pressure interpolation, and the first-order up-wind difference scheme is adopted for discretizing momentum equation and energy equation. The courant number can be defined as the ratio of the time step to the time a fluid takes to move over a cell, which must be not excessed 250. According to convergent solution, the time step 10^{-4} s is selected to obtain the solution and solve all above equations, which gave convergent solution and Courant number be less than 3.

Vapor and liquid phases were known as primary and secondary phases respectively. The water liquid density and the effect of polynomial equations of surface tension at interaction between the multi-phases are included as following [24].

For the surface tension

$$\sigma_{LV} = 0.09805856 - 1.845 \times 10^{-5}T - 2.3 \times 10^{-7}T^2 \quad (22)$$

For water liquid density

$$\rho_L = 859.0083 + 1.252209 T - 0.002649T^2 \quad (23)$$

Where T is the temperature in kelvin.

The solution for this study is converged when the residual of the momentum equation is less than 10^{-4} and the courante number obtained due to the time step is less than 3. The iteration convergent history is shown in Figure 6.

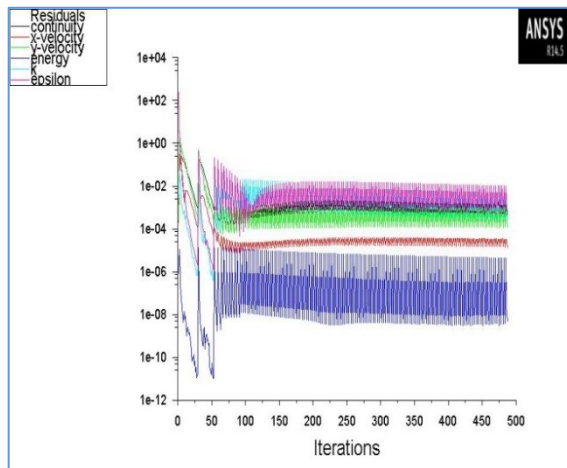


Figure 6: Convergent solution

5. Error Analysis

The root-sum-square (RSS) approach was used for many thermal engineering laboratory report data analysis [25]. The calculations of thermal resistance and heat transferred to the evaporator section are the main source of uncertainty that came from the temperature and air velocity readings.

The propagation of uncertainties related to calculations of heat of evaporator section values ($S_{Q_{in}}$) as below:

$$\frac{S_{Q_{in}}}{Q_{in}} = \sqrt{\left(\frac{S_{(T_i-T_o)}}{T_i-T_o}\right)^2 + \left(\frac{S_u}{u}\right)^2} \quad (24)$$

$$S_{(T_i-T_o)} = \sqrt{S_{T_i}^2 + S_{T_o}^2} \quad (25)$$

And for thermal performance:

$$\frac{S_{R_{th}}}{R_{th}} = \sqrt{\left(\frac{S_{(T_{eva}-T_{con})}}{T_{eva}-T_{con}}\right)^2 + \left(\frac{S_{Q_{in}}}{Q_{in}}\right)^2} \quad (26)$$

Where

$$S_{(T_{eva}-T_{con})} = \sqrt{S_{T_{eva}}^2 + S_{T_{con}}^2} \quad (27)$$

The maximum uncertainty associated with the resulting Q_{in} and R_{th} values was found to be around 6%.

6. Results and Discussions

I. Experimental results

Test results of air temperature vs. heating power of various face velocity for OHP are plotted in Figure 7. This figure showed the effect of hot-air temperature on the heat-transfer rate to the evaporation section. It can be seen that the heating power input to the evaporator section increased with increasing the air inlet temperature with all air face velocity. The heat input has the same trend for all velocities. The maximum heat input is 107 W achieved at velocity 1.5 m/s and temperature 50 °C while the minimum heat input is 13.75 W at 35 °C at velocity 0.5 m/s.

Figure 8 presented the effect of air inlet temperature on thermal resistance. The thermal resistance of OHP decreases rapidly by about 60.8% at 0.5 m/s and decreased about 51.2% at 1m/s and by 56.3% at 1.5m/s due to the increase in heat input as shown in Figures 9, 10, and 11 respectively. The results were recorded minimum thermal resistance 0.2312 °C/W at 107.75 W and maximum thermal resistance 1.036°C/W at 13.75 W. These experimental results are agree with previous work [26,12].

The thermal resistance at lower heat input affected reversely by gravity on the performance and pulsations flow behavior. On the other hand, the revers effect of gravity can be overcome by further addition of heat. This is due to the increase of heat input that will lead to improving performance and sustained pulsation flow of OHP. Therefore, a higher circulation rate of the working fluid has occurred which results in heat transfer enhancement.

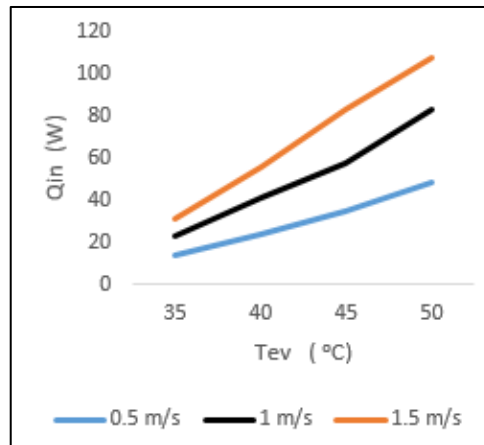


Figure 7: Power heat input vs hot air inlet temperature of various face velocity

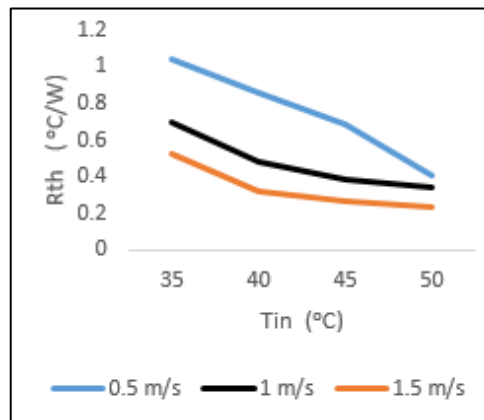


Figure 8: Thermal resistance vs hot air inlet temperature of various face velocity

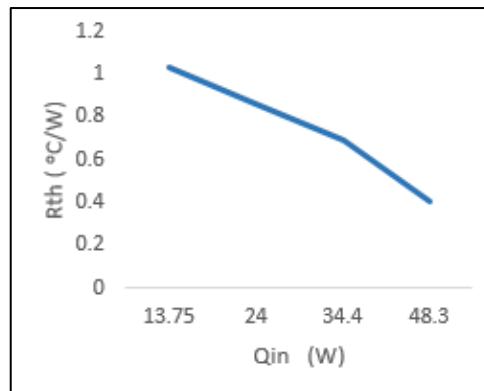


Figure 9: Thermal resistance vs evaporator heat input at 0.5 m/s air face velocity

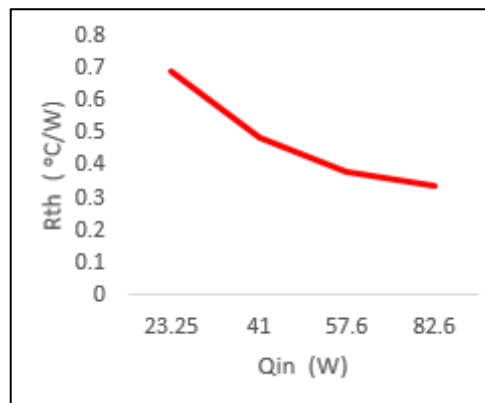


Figure 10: Thermal resistance vs evaporator heat input at 1m/s air face velocity

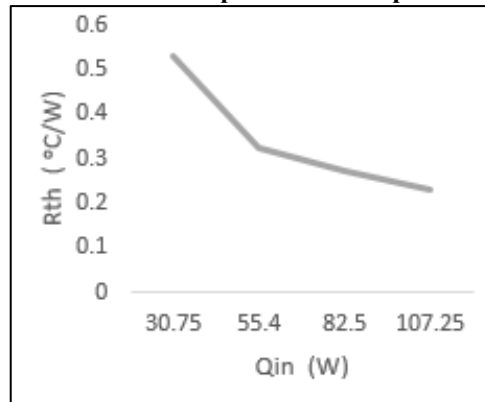


Figure 11: Thermal resistance vs evaporator heat input at 1.5 m/s air face velocity

The thermal conductivity illustrated in Figure 12. The increasing of air input temperature led to increasing in the effective thermal conductivity at all considering air face velocity. This behavior of thermal conductivity has been confirmed with some experimental work like [4, 11]. The increase in the thermal conductivity is due to the heat transferred by working fluid inside the OHP from the evaporator section to the condenser section by working fluid also increased according to latent heat absorption and dissipation processes in both sections.

II. The numerical results

The simulation run is consuming 90 computer working days to gate simulation results for 60 seconds. The numerical results showed for vertical mode, the greatest amount of liquid slugs located in the bottom of channels because of the effect of gravity at time 0 s. When heating power continuously occurred, Figure 13 shows bubbles would first appear in the sidewall of channels. After time 0.04 sec, the local nucleation started and vapor bubbles will begin to generate on the small cavities of walls in the bottom of the evaporator section. The nucleation process starts when the temperature of the internal wall of the evaporator section was greater than the saturated temperature of the working fluid.

The increasing of evaporator section temperature led to an increase in the growth rate of bubbles as shown in Figure 14. Vapor bubbles growing up as mentioned and the vapor bubbles will try to separate from the wall, rise to the upper regions, grew quickly and coalesced to form vapor plugs. This will induce the flow pattern transition from dispersed bubbles pattern to the vapor slug pattern. Therefore, the liquid volume fraction decreased. The heating and evaporation process of working fluid resulted in pressure imbalance, which generates the oscillation motion.

The contours of temperature distribution along the wall of the OHP have been recorded at different times including the start-up heating process to understand the process of heat transfer through the operation of OHP. In this visual observation, the temperature distribution in the working fluid region inside the condenser section, evaporator section, and adiabatic section also recorded.

Figure 15, at time 0 s the temperature of OHP with water working fluid initially at 300 K because the operation condition not applied yet. The contours of temperature showed the vapor plug temperature change with a time step change in the operation of OHP. This changing in temperature is recorded,

that specify the heat transfer process. With time increased, the temperature in the evaporation section increased because power input is continued, the temperature distribution at time 0.1 s as shown in Figure 16 that visualize the expanded of the hot region from the evaporator section to the condenser section. This is because of the continued supplying of input heat power in the evaporation section of OHP, the acceleration of bubbles growth is increased and the next bubbles were accelerated to catch up with the previous bubble. So some initial tiny spherical bubbles merged into a large vapor column and then the bubbles jetted through the evaporation section to the condensation section through the adiabatic section, where the flow pattern was divided into the liquid and vapor phase in the axial direction. These results in the high-temperature region expanded due to the volume expansion of the vapor plug from (0.1 s) to (1 s). Figure 17 showed the maximum and minimum temperature distribution of two-phase flow inside OHP at different times. The temperature distribution of the working fluid inside the OHP became more uniformly at time 60 s as shown in Figure 17.

The predicted simulation results of CFD vs. the experimental results are plotted in Figure 18. As shown in Figure 18, the theoretical evaporator section temperature results had the same trend and better agreement with the experimental results. The experimental average wall temperature of the evaporator section has deviated from the theoretical results by maximum average relative error about 15% may be due to the consideration of convection and conduction heat losses taking place at condenser and evaporator section.

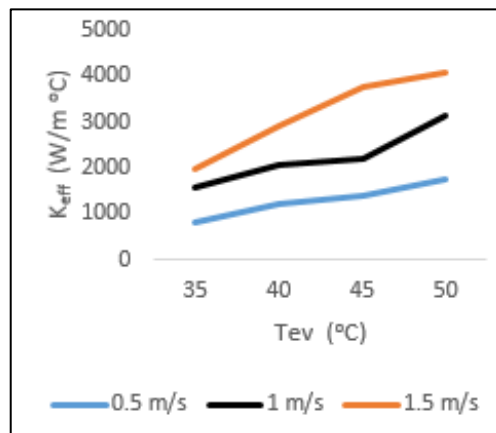


Figure 12: Thermal conductivity vs hot air inlet temperature of various face velocity

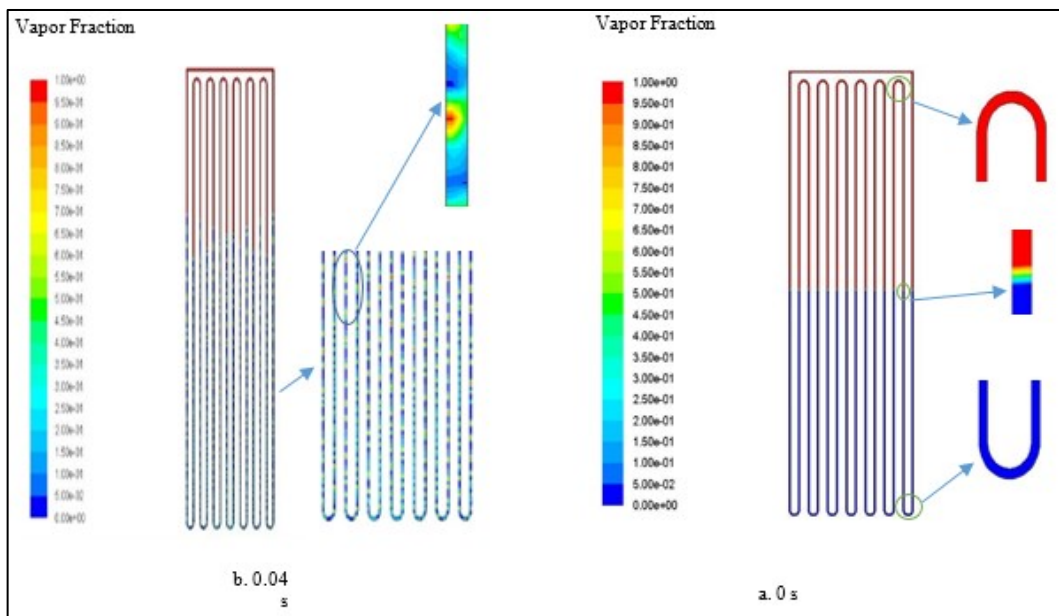


Figure 13: Contours of vapor Fraction at different time. a. at 0 s, b. at 0.04 s

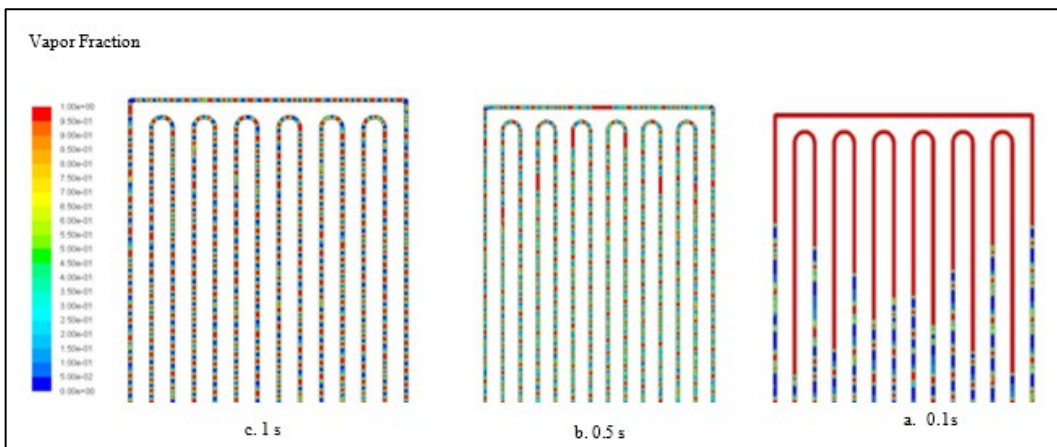


Figure 14: Contours of vapor Fraction at different time. a. at 0.1s, b. at 0.5 s and c. at 1.0 s.

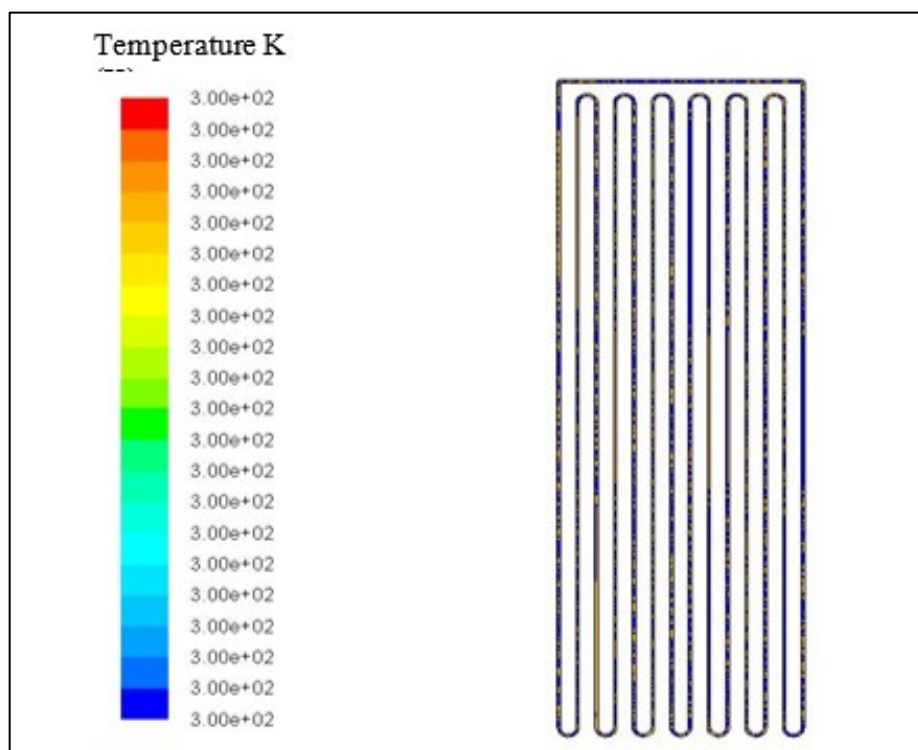
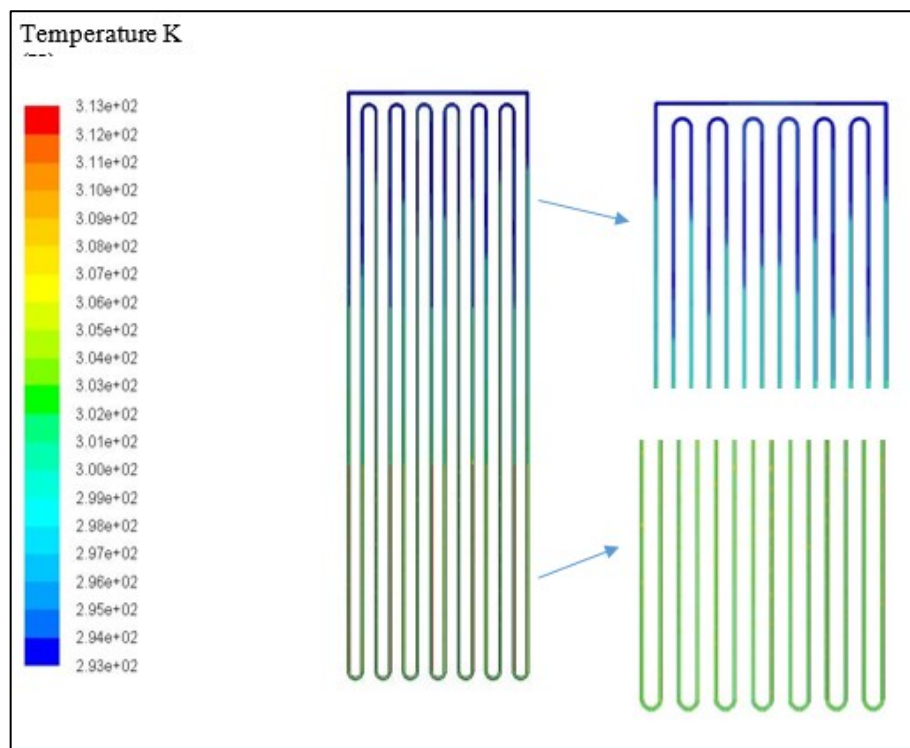
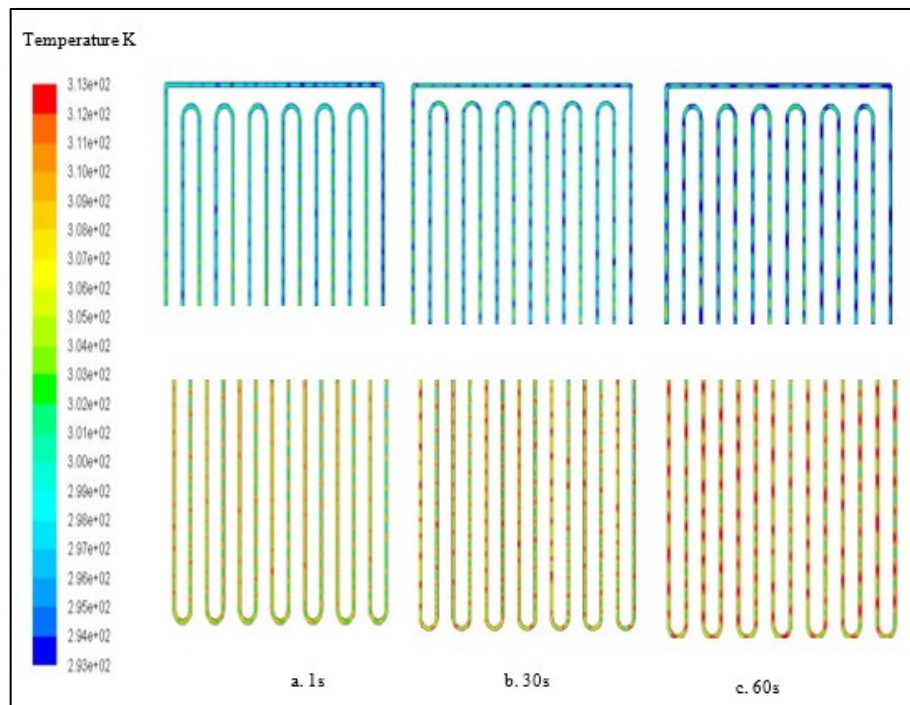


Figure 15: Contour of temperature wall distribution at time 0s.

**Figure 16: Contour of temperature wall distribution at time 0.4s.****Figure17: Contours of temperature wall distribution at different time. a. at 1s, b. at 30s and c. at**

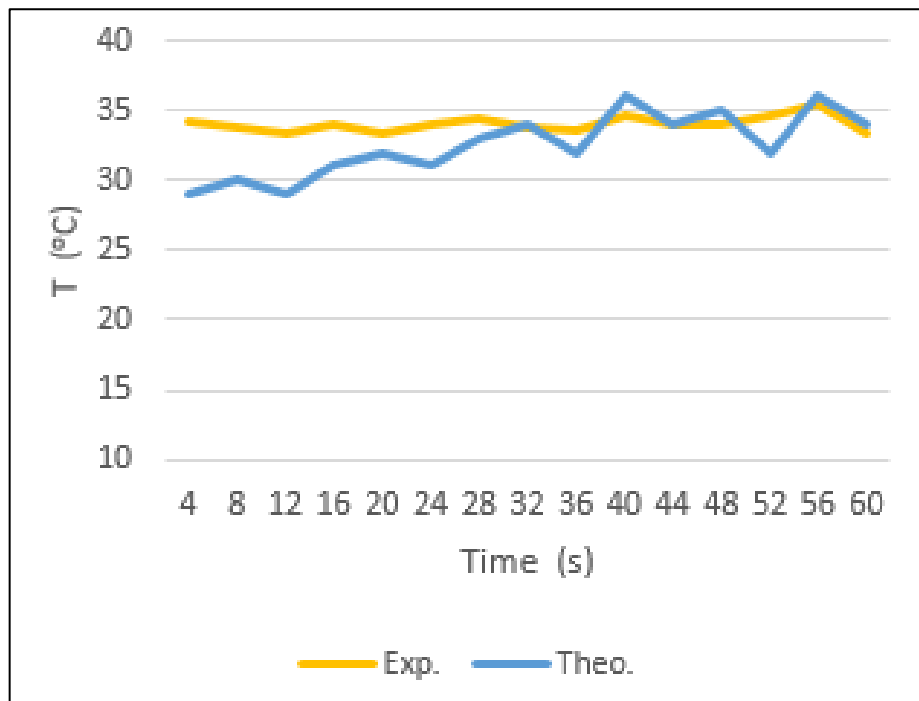


Figure 18: Average wall evaporator temperature comparison between experimental and CDF results

7. Conclusions

The OHP thermal performance is characterized by different hot air inlet temperature with different face velocity by thermal resistance and effective thermal conductivity. The experimental results showed that increasing the air temperature would also increase the heating power inputs, which leads to enhance the thermal performance of OHP.

Simulation CFD with VOF model can simulate the complex two-phase flow phenomena inside the OHP successfully by prediction the evaporation and condensation process in OHP. In the same condition, the comparison between experimental results and CFD results had been conducted. The predicted results showed quite well agree with the experimental results.

Nomenclature

OHP = oscillation heat pipe.

VOF = Volume of fluid.

CLOHP/CV = closed loop OHP with check valve.

CFD = computational Fluid Dynamics.

UDF= user defined function.

Q_{in} = heat input, W.

C_p = specific heat, J/kg.K.

R_{th} = thermal resistance, °C/W.

T_i = temperature in, °C.

Subscripts

l = liquid.

v = vapor.

e = evaporator.

c = condenser.

sat = saturation

References

- [1] Y. Zhang, A. Faghri, M.B. Shafii, "Analysis of liquid-vapor pulsating flow in a Ushaped miniature tube," Int. J. Heat Mass Transfer, 45, 12, 2501–2508, 2002.
- [2] H.B. Ma, B. Borgmeyer, P. Cheng, et al., "Heat transport capability in an oscillating heat pipe," Journal Heat Transfer, 130, 081501-1–081501-7, 2008.
- [3] S.B. Liang, H.B. Ma, "Oscillating motions of slug flow in capillary tubes," Int. Comm. Heat Mass Transfer, 31, 3, 365–375, 2004.
- [4] S. M. Thompson, B. S. Tessler, H. B. Ma, D. E. Smith and A. Sobel, "Ultra-High Thermal Conductivity of Three-Dimensional Flat-Plate Oscillating Heat Pipes for Electromagnetic Launcher Cooling," Proceedings of IEEE 16th International Symposium on Electromagnetic Launch Technology, 2012.
- [5] Y .H. Yau, "The heat pipe heat exchanger: a review of its status and its potential for coolness recovery in tropical buildings," Building Serv. Eng. Res. Technol. 29, pp. 291–310, 2008.
- [6] A. J. Jiao, H. B. Maa, J. K. Critser, "Experimental investigation of cryogenic oscillating heat pipes," International Journal of Heat and Mass Transfer 52, 3504–3509, 2009.
- [7] D. WANG, Xiaoyu. CUI, "Experiment research on pulsating heat pipe with different mixtures working fluids," The 21st International Symposium on Transport Phenomena, 2-5, 2010.
- [8] N. Bhuwakietkumjohn and Th. Paramethanuwat, "The top heat mode of closed loop oscillating heat pipe with check valves at the top heat mode (THMCLOHP/CV): a thermodynamic study," International Journal of Mechanical and Materials Engineering, 2014.
- [9] G. Mahajan, H. Cho, S. M. Thompson, H. Rupp and K. Muse, "Oscillating heat pipes for waste heat recovery in HVAC systems," Proceedings of the ASME, 13-19, 2015.
- [10] M L. Rahman, Sumaiya Nawrin, and Rasel A Sultan, Fariha Mir, and Mohammed Ali, "Effect of fin and insert on the performance characteristics of close loop pulsating heat pipe CLPHP," Procedia Engineering 105, 129 – 136, 2015.
- [11] J. Qu, X. Li, Q. Xu and Q. Wang, "Thermal performance comparison of oscillating heat pipes with and without helical micro-grooves," Heat Mass Transfer, Vol. 53, Issue 11, pp 3383–3390, 2017.
- [12] M. A. Nazaria, R. Ghasempoura, M. H. Ahmadib, Gh. Heydarianc, M. B. Shafiic, "Experimental investigation of graphene oxide nanofluid on heat transfer enhancement of pulsating heat pipe," International Communications in Heat and Mass Transfer, 91, 90–94, 2018.
- [13] Z. Lin, Sh. Wang, R. Shirakashi, L. W. Zhang, "Simulation of a miniature oscillating heat pipe in bottom heating mode using CFD with unsteady modeling," International Journal of Heat and Mass Transfer 57: 642–656, 2013.
- [14] S. Y. Nagwase, P. R. Pachghare, "Experimental and CFD Analysis of Closed Loop Pulsating Heat Pipe with DI-Water," IEEE 1, 185 – 190, 2013.
- [15] H. Jouhara and R. Meskimmon, "Experimental investigation of wraparound loop heat pipe heat exchanger used in energy efficient air handling units," Energy, 35, 4592-4599, 2010.
- [16] M. B. Shafii, A. Faghri and Y. Zhang, "Thermal Modeling of Unlooped and Looped Pulsating Heat Pipes," Journal of Heat Transfer, Vol. 123/ 1159, 2001.
- [17] K. Morris, "An Experimental Investigation of The Heat Transfer Capability and Thermal Performance of Dual Layer Pulsating Heat Pipes," Msc. thesis University of Rhode Island, 2012.
- [18] D. D. Tung and S. Torii, "Heat Transfer Performance of a Self-Oscillating Heat Pipe Using Pure Water and Effect of Inclination to This Performance," ASEAN Engineering Journal, Vol 2 No 1, ISSN 2586, 9159 p. 93, 2012.
- [19] T. M. Sathe and U. S. Wankhede, "Review on Closed Loop Oscillating Heat Pipe," International Journal of Engineering Research & Technology (IJERT), Vol. 3 Issue 3, 2014.
- [20] S. Khandekar, P. Charoensawan, M. Groll, P. Terdtoon, "Closed loop pulsating heat pipes Part B: visualization and semi-empirical modeling," Applied Thermal Engineering 23, 2021–2033, 2003.
- [21] ANSYS FLUENT, Theory Guide (Release 13.0). Multiphase Flows, ANSYS, Inc.', pp. 455-568 (chapter 17), 2010.

- [22] J.U. Brackbill, D. B Kothe and C Zemach, "A continuum method for modeling surface tension," *Journal of Computational Physics*, Volume 100, Issue 2: Pages 335-354, 1999.
- [23] S. C. K. De Schepper, G. J. Heynderickx, G. B. Marin, "Modeling the evaporation of a hydrocarbon feedstock in the convection section of a steam cracker," *Computers & Chemical Engineering* 33: 122- 132, 2009.
- [24] B. Fadhl, L. C. Wrobel, H. Jouhara, "Numerical modeling of the temperature distribution in a two-phase closed thermosyphon," *Applied Thermal Engineering*, 60, 122-131, 2013.
- [25] J.R. Taylor, "An Introduction to Error Analysis: The Study of Uncertainties in Physical Measurements," University Science Books, Sausalito, 1997.
- [26] K. H. Chien, Y. T. Lin, Y. R. Chen, K. Sh. Yang, C. Ch. Wangc, "A novel design of pulsating heat pipe with fewer turns applicable to all orientations," *International Journal of Heat and Mass Transfer* 55, 5722– 5728, 2012.